

Wavelength and Mode Division Multiplexer Working in Communication Bands for TE0 and TM0 Modes Based on LNOI Platform

Mengyao Zhao¹, and Jianji Dong^{1,*}

¹Wuhan National Laboratory for Optoelectronics, Huazhong University of Science and Technology, Wuhan, 430074, Hubei, China

*Corresponding author. Email: jjdong@hust.edu.cn

Abstract—We propose a wavelength and mode division multiplexer based on lithium niobate-on-insulator platform. The multiplexer can separate the transverse magnetic and transverse electric fundamental modes at 1310 nm and 1550 nm simultaneously.

Keywords—Lithium niobate-on-insulator, wavelength division multiplexer, polarization splitter-rotator, mode division multiplexer

I. INTRODUCTION

Lithium niobate (LN) has large transparency window, relatively high refractive index and excellent nonlinear properties [1]. In recent years, a variety of integrated optical devices have been successfully achieved on the lithium niobate-on-insulator (LNOI) platform, including electro-optical modulators [2], high quality resonators [3], polarization splitter-rotators [4, 5], and optical filters [6]. Communication systems typically use light at 1550 nm and 1310 nm as carriers, while mode division multiplexing is used to improve the efficiency of information transmission.

In this work, we present a wavelength division multiplexer (WDM) that operates at 1550 nm and 1310 nm, and also functions as a mode division multiplexer (MDM) due to its capability to separate the fundamental transverse magnetic mode (TM0) and fundamental transverse electric mode (TE0).

II. PRINCIPLE AND DESIGN

Fig. 1 depicts the schematic of the proposed device, which consists of an adiabatic taper, two asymmetrical directional couplers (ADC) and a multimode interference (MMI). The device is designed on a X-cut LNOI wafer with a 360 nm LN film thickness, and the input light mainly propagates along the Y-axis of LN. When inputting TE0 modes at both 1310 nm and 1550 nm, and TM0 modes at both 1310 nm and 1550 nm simultaneously, the light will output from port 3, port 2, port 1, and port 4, respectively. Notably, the energy of TM0 modes will convert into TE0 modes after passing through the ADCs and ultimately output in the form of TE0 modes.

Fig. 2(a) displays the cross section of the waveguide, and the parameters defined in Fig. 1 and Fig. 2(a) are designed as follows: $w_1 = 1 \mu\text{m}$, $w_2 = 1.3 \mu\text{m}$, $w_3 = 2 \mu\text{m}$,

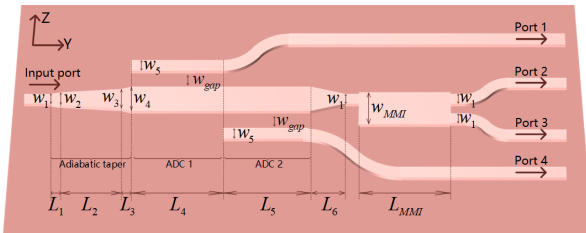


Fig. 1. The schematic of the proposed device.

$w_4 = 2.5 \mu\text{m}$, $w_5 = 1.1 \mu\text{m}$, $w_{\text{gap}} = 0.425 \mu\text{m}$, $w_{\text{MMI}} = 3 \mu\text{m}$, $L_1 = 5 \mu\text{m}$, $L_2 = 320 \mu\text{m}$, $L_3 = 35 \mu\text{m}$, $L_4 = 130 \mu\text{m}$, $L_5 = 66 \mu\text{m}$, $L_6 = 25 \mu\text{m}$, $L_{\text{MMI}} = 146.5 \mu\text{m}$, $h_{\text{slab}} = h_{\text{etch}} = 180 \text{ nm}$, $h_{\text{clad}} = 1.5 \mu\text{m}$, $\theta = 60^\circ$. The effective indices of the first three eigenmodes at 1310 nm and 1550 nm are calculated and presented in Fig. 2(b) and (c), respectively. The dotted circles in Fig. 2(b) and (c) indicate that the TM0 mode and TE1 mode will experience hybridization when the waveguide width varies from 1.3 μm to 2 μm , and this process can be adiabatic if the taper is sufficiently long. The dotted lines in Fig. 2(b) and (c) show that the TE0 mode in a 1.1 μm -width waveguide and the TE1 mode in a 2 μm -width waveguide have equal effective indices, ensuring the potential coupling between the two modes mentioned above.

To determine the optimal length of the adiabatic taper, the simulations are performed to calculate the mode

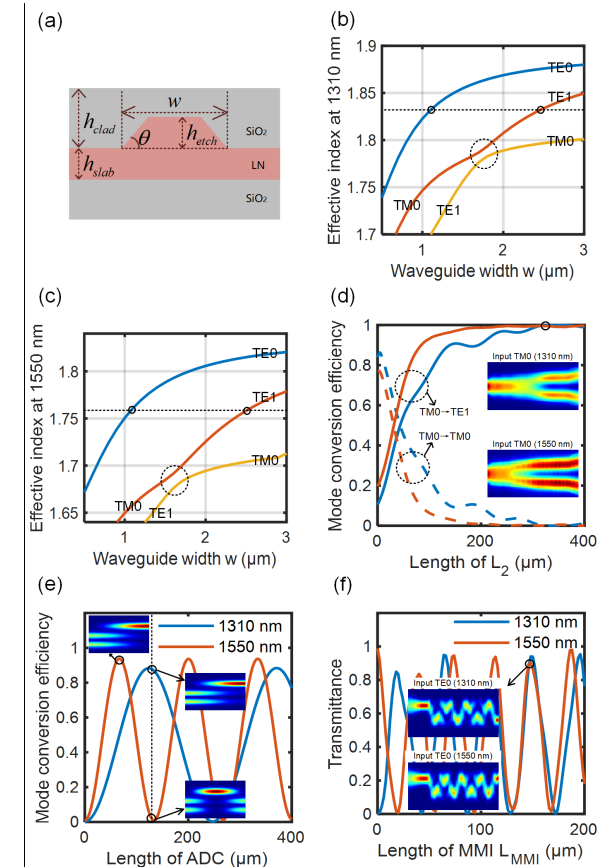


Fig. 2. The parameter design of each part. (a) Cross section of the waveguide. (b) Effective indices of the first three eigenmodes at 1310 nm. (c) Effective indices of the first three eigenmodes at 1550 nm. (d) The mode conversion efficiency of TM0 to TE1 mode and TM0 to TM0 mode as a function of taper length L_2 . Blue curves represent the results at 1310 nm and red curves represent results at 1550 nm. (e) Mode conversion efficiency between two adjacent waveguides as a function of length of ADC. (f) Transmittance of TE0 mode at 1310 nm and 1550 nm as a function of length of MMI L_{MMI} .

conversion efficiencies for different values of L_2 . As shown in Fig. 2(d) and labeled by a black circle, when $L_1 = 5 \mu\text{m}$, $L_2 = 320 \mu\text{m}$, $L_3 = 35 \mu\text{m}$, more than 99.5% of the energy of the TM0 modes is converted to TE1 modes at both 1310 nm and 1550 nm. The simulation results of light propagation are shown as insets in Fig. 2(d), with blue curves representing the results at 1310 nm and red curves representing results at 1550 nm. Since no mode hybridization occurs with the TE0 mode, the TE0 mode at both wavelengths remains unchanged in the adiabatic taper.

The lengths of two ADCs are finalized by considering the mode coupling between two adjacent waveguides, whose widths are decided according to the dotted lines in Fig. 2(b) and (c). According to the simulation results shown in Fig. 2(e), the length of ADC 1, which is L_4 , is designed to be 130 μm to maximize the coupling efficiency of the TE1 mode at 1310 nm and minimize the coupling efficiency of the TE1 mode at 1550 nm. Similarly, the length of ADC 2, which is L_5 , is chosen to be 66 μm to maximize the coupling efficiency of the TE1 mode at 1550 nm between two adjacent waveguides. After propagating through ADCs, the majority of the energy of the TE1 modes at 1310 nm and 1550 nm will exit the central waveguide and be output from port 1 and port 4, respectively.

The optimal length of MMI is determined based on the simulation results presented in Fig. 2(f). The curves in this figure indicate that the TE0 mode at both 1310 nm and 1550 nm will achieve a relatively high transmittance when the length of the MMI is set to be 146.5 μm .

III. RESULTS

After finalizing the values of each parameter, the light propagation throughout the entire structure is simulated. The top views of light power when different modes are input at both 1310 nm and 1550 nm are plotted in Fig. 3. The figure shows that the proposed structure is capable of functioning as a WDM and MDM simultaneously. Fig. 4 demonstrates the simulation performance of the device for the O-band, S-band, and C-band communication wavelength. The results show that the energy output from the target port is approximately 10 dB larger than that of

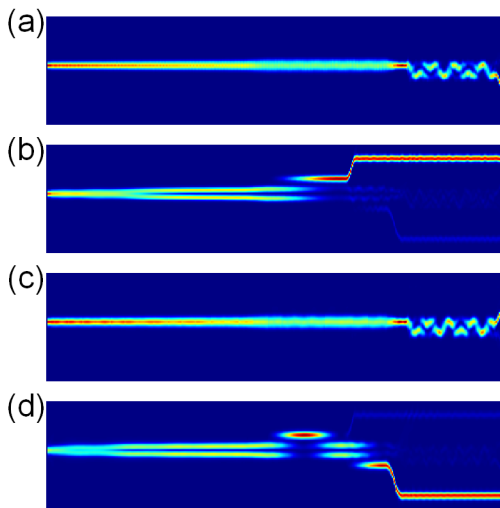


Fig. 3. The light propagation throughout the entire structure when (a) TE0 mode at 1310 nm, (b) TM0 mode at 1310 nm, (c) TE0 mode at 1550 nm, and (d) TM0 mode at 1550 nm input from the input port.

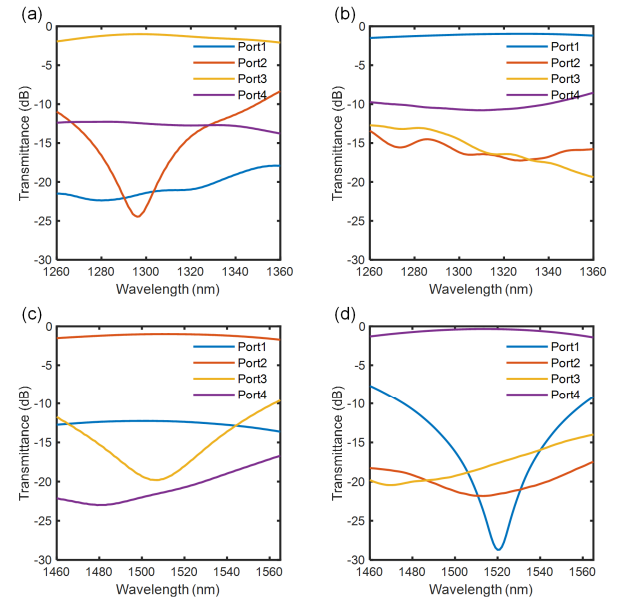


Fig. 4. Simulated transmittance at each output port when (a) TE0 mode in O-band, (b) TM0 mode in O-band, (c) TE0 mode in S-band and C-band, and (d) TM0 mode in S-band and C-band input from the input port.

other ports, proving that the structure can operate effectively across a wide range of wavelengths.

IV. CONCLUSION

Based on the principles of mode coupling and multimode interference, we have successfully demonstrated an integrated structure on the LNOI platform that functions as both a WDM and a MDM for TE0 and TM0 modes in the O-band, S-band, and C-band wavelengths. The device demonstrates a high extinction ratio of over 10 dB between different ports according to the simulation results. Our work has the potential for improving information transmission efficiency when the integrated devices on the LNOI platform work in the communication bands.

ACKNOWLEDGMENT

This work was partially supported by the National Key Research and Development Project of China (2022YFB2804200), the National Natural Science Foundation of China (U21A20511), the Innovation Project of Optics Valley Laboratory (Grant No. OVL2021BG001).

REFERENCES

- [1] G. Chen *et al.*, "Advances in lithium niobate photonics: development status and perspectives," *Advanced Photonics*, vol. 4, no. 03, 2022, doi: 10.11117/1.Ap.4.3.034003.
- [2] C. Wang *et al.*, "Integrated lithium niobate electro-optic modulators operating at CMOS-compatible voltages," *Nature*, vol. 562, no. 7725, pp. 101-104, Oct 2018, doi: 10.1038/s41586-018-0551-y.
- [3] J. D. Witmer, J. A. Valery, P. Arrangoiz-Ariola, C. J. Sarabalis, J. T. Hill, and A. H. Safavi-Naeini, "High-Q photonic resonators and electro-optic coupling using silicon-on-lithium-niobate," *Sci Rep*, vol. 7, p. 46313, Apr 13 2017, doi: 10.1038/srep46313.
- [4] H. Z. Luo *et al.*, "High-Performance Polarization Splitter-Rotator Based on Lithium Niobate-on-Insulator Platform," (in English), *Ieee Photonic Tech L*, vol. 33, no. 24, pp. 1423-1426, Dec 15 2021, doi: 10.1109/Lpt.2021.3123101.
- [5] X. H. Wang, A. Pan, T. A. Li, C. Zeng, and J. S. Xia, "Efficient polarization splitter-rotator on thin-film lithium niobate," (in English), *Optics Express*, vol. 29, no. 23, pp. 38044-38052, Nov 8 2021, doi: 10.1364/Oe.443798.

- [6] Y. Ding *et al.*, "Thermo-optic tunable optical filters with GHz-bandwidth and flat-top passband on thin film lithium niobate platform," *Optics Express*, vol. 30, no. 12, 2022, doi: 10.1364/oe.458218